Acta Materialia 79 (2014): 181 - 187

DOI: http://dx.doi.org/10.1016/j.actamat.2014.06.040

Band-gap engineering of $Cu_2ZnSn_{1-x}Ge_xS_4$ single crystals and influence of the surface properties

R.Caballero[*,a], I. Victorov[b], R. Serna[c], J. M. Cano-Torres[a], C. Maffiotte[d], E.Garcia-Llamas[a], J. M. Merino[a], M. Valakh [e], I. Bodnar[b], M. León[a]

[a]Universidad Autónoma de Madrid, Departamento de Física Aplicada, C/ Francisco Tomás y Valiente 7, 28049 Madrid, Spain

[b]Belarusian StateUniversity of Informatics and Radioelectronics, P. Brovka 6, 220013 Minsk, Belarus

[c]Instituto de Óptica Daza de Valdés, CSIC, C/ Serrano 121, 28006 Madrid, Spain

[d]CIEMAT, Departamento de Tecnología, Avd. Complutense 40, 28040 Madrid, Spain

[e]V. Lashkaryov Institute of Semiconductor Physics of National Academy of Sciences of Ukraine, 41 Prospect Nauky, 03028 Kyiv, Ukraine

Corresponding Author*raquel.caballero@uam.es, Tel: +34 914978559, Fax: +34 914973969

ABSTRACT. Thin film solar cells based on $Cu_2ZnSn(S,Se)_4$ are very promising due to the fact that they contain earth-abundance elements and show a high absorptivity. However, the performance of these solar cells needs to be improved in order to reach efficiencies as high as that reported for $Cu(In,Ga)Se_2$ –based devices. Here we investigate the potential of band-gap engineering of $Cu_2ZnSn_{1-x}Ge_xS_4$ single crystals grown by chemical vapour transport as a

function of the [Ge]/([Sn]+[Ge]) atomic ratio. The fundamental band gap E_0 is found to change from 1.59 to 1.94 eV when the Ge content is increased from x = 0.1 to 0.5 as determined from spectroscopic ellipsometry measurements. This knowledge opens a route to enhance the performance of kesterite-based photovoltaic devices by a Ge-graded absorber layer. Furthermore, the formation of GeO_2 on the surface of the as-grown samples was detected by X-ray photoelectron spectroscopy, having an important impact on the effective optical response of the material. This should be also taken into account when designing photovoltaic solar cells.

KEYWORDS. Kesterite; Germanium; GeO_2; spectroscopic ellipsometry; solar cells

1. Intoduction

$Cu_2ZnSn(S,Se)_4$ (CZTSSe) is a very promising material for the absorber layer of thin film solar cells due to its earth-abundant composition, excellent optical properties and outstanding performance. A 12.6 % efficiency has been recently achieved for CZTSSe solar cells performed using a hydrazine-based pure solution approach [1]. Other different chemical and physical methods have been used for the preparation of CZTSSe thin films [2-11]. Among them, an efficiency of 9.2% has been reported on 5 x 5 cm^2–sized Cu_2ZnSnS_4 (CZTS) submodule by annealing of metal precursors [6] and 8.4 % for pure CZTS grown by thermal evaporation at 150º C and subsequent 570º C hot-plate annealing at atmospheric pressure [7]. However, the highest efficiency is still below the physical Schockley-Queisser limit of about 31 % efficiency under terrestrial conditions [12]. Moreover, the highest 12.6 % performance is also far away from the 20.8% achieved for $CuIn_{1-x}Ga_xSe_2$ (CIGSe) thin film solar cells [13].

The ability to adjust the optical band-gap energy of the absorber layer is critical for optimizing the performance of photovoltaic devices. The success of CIGSe solar cells is mainly based on the absorber band-gap engineering [14]. A Ga gradient through the absorber layer has been shown as a key issue to enhance the photovoltaic parameters of CIGSe cells [15-16]. A similar strategy can be applied to the CZTSSe material by alloying with Ge. CZTSSe compound has a crystal structure similar to that of CIGSe, with direct optical transition and p-type semiconductor behaviour [17]. From first principles calculations it has been shown that for Cu_2ZnSnS_4 (CZTS) (Cu_2ZnGeS_4 (CZGS)) and $Cu_2ZnSnSe_4$ (CZTSe) ($Cu_2ZnGeSe_4$ (CZGSe)) the conduction band minimum (CBM) is mainly formed by anti-bonding Sn (Ge) *s* and anion *p* hybrid orbitals, while the valance band maximum (VBM) mainly involves the hybridization of Cu *d* and anion *p* orbitals [18-19]. Therefore, replacing Sn with smaller Ge atoms should strengthen the *s*-*s* and *s*-*p* level repulsion between Ge and

S/Se atoms that would result in an increased anti-bonding character of the CBM. Therefore, it is expected an increase of the fundamental band gap energy value by replacing Sn by Ge. Guo et al. [20] have reported an enhancement of the performance of CZTSSe solar cells, from 7.2 % to 8.4 %, by partial substitution of Sn by Ge. This improvement was mainly due to a higher open circuit voltage, V_{oc}, and fill factor, FF. Moreover, the higher band-gap energy obtained by adding Ge also offers the possibility of using CZTGS as absorber layer of a top cell for a tandem device.

The goal of this work is to investigate the fundamental gap and the different energy transitions of $Cu_2ZnSn_{1-x}Ge_xS_4$ ($CZT_{1-x}G_xS$) single crystals with different Ge contents (x = [Ge]/([Ge]+[Sn] = 0.1, 0.5) by means of spectroscopic ellipsometry. We consider this point very important to design the appropriate Ge-graded depth profile to achieve an enhancement of the CZTGS solar cell performance. Moreover, the surface material composition is studied by X-ray photoelectron spectroscopy (XPS), and its influence on the optical performance is determined.

2. Experimental

2.1. Single crystal growth

The crystals were grown by chemical vapour transport (CVT) of the elements using iodine as a transport agent [21]. Before the CVT growth, the CZTGS compound was synthesized by a modified Bridgman method. For the CVT process, a quartz ampoule was filled with the ground compound adding 5 mg/cm^3 of Iodine. The ampoule was placed in a two-zone furnace, in a way that reaction zone temperature was around 80 K higher than that of the crystallization zone. Afterwards, temperature was increased up to 1053 K (≈ 973 K in crystallization zone) and was maintained there for 8 days.

Three samples were studied: one sample with x approximately of 0.1, $CZT_{0.9}G_{0.1}S$-1, and other two with x ≈ 0.5 but with different Zn and Cu contents, $CZT_{0.5}G_{0.5}S$-1 and -2. There were no significant differences between the precursors used for the growth processes 1 and 2. Small temperature variations (± 10 K) during crystal growth could explain the different composition for the samples $CZT_{0.5}G_{0.5}S$-1 and -2. As a minor effect, a small deviation in Iodine concentration could also take place (± 2 %).

2.2. Single crystal characterization

The crystals were investigated by X-ray diffraction (XRD). Powder XRD difractograms were recorded in a X´Pert PRO Θ-2Θ equipment operating in Bragg-Brentano geometry using Cu K_α radiation. Laue X-ray back reflection was used to confirm the high quality of the single crystals (not shown here). In addition, Micro-Raman spectroscopy measurements were performed to obtain deeper information about the structure of the crystals. Raman spectra were obtained at room temperature in a Horiba Jobin Ivon T64000 spectrometer. The laser wavelength was adjusted to 514.5 nm with a spot size of 0.7 μm of diameter. The measurement of the spectroscopic ellipsometry parameters ψ and δ of the crystals was carried out with a variable angle spectroscopic ellipsometer (Woollam VASE) at room temperature at three incidence angles of 60º, 65º and 70º, in the photon energy range from 0.75 eV to 4.5 eV using 0.025 eV steps. XPS measurements were performed with a Perkin-Elmer PHI 5400 spectrometer equipped with a Mg K_α excitation source (hν = 1253.6 eV). The beam size was of 1 mm diameter. The different photoemission contributions have been fitted by Voigt functions and a linear background.

The composition of the samples was measured by Energy Dispersive X-ray (EDX) (Oxford instruments, model INCAx-sight) inside a Hitachi S-3000N scanning electron microscope. EDX measurements were carried out at 25 kV operating voltage and the Cu K, Zn K, Sn L,

Ge K and S K lines were used for quantification. Table 1 shows the composition of the samples investigated. As shown in Table 1, the main difference between the last two samples is the Cu, Zn and S contents. The results shown in Table 1 are an average of five measurements in different points of the samples. The relative error of the concentration values is of maximum 1 %.

3. Results

The efficiency of CZTS solar cells is also determined by the structural feature of this material. This compound can be formed in two crystallographic structures, kesterite (space group I 4) and stannite (space group I 42 m), which present different band gap energies [17]. Here the structure of the CZTGS single crystals has been investigated by XRD and Raman spectroscopy. Figure 1 displays the XRD spectra of $CZT_{0.9}G_{0.1}S$-1 and $CZT_{0.5}G_{0.5}S$-1 single crystals. JCPDS reference data for tetragonal kesterite CZTS (01-075-4122) and tetragonal stannite CZGS (04-012-7580) are also shown. Both crystals show a tetragonal structure. Figure 2 shows the Raman spectra of the same samples. In both XRD and Raman spectra, it is observed a shift of several diffraction peaks towards higher angles and Raman modes towards higher wavenumbers when Ge content increases. This fact evidences the structural compositional changes.

Different optical properties of CZTS [22] and CZGS [23] bulk crystals have been already investigated, but so far there is no information on the dielectric function of the CZTGS solid solution. As explained in [24], the preparation of a good quality surface of the material is extremely important in order to minimize the surface roughness and oxide formation effects. Therefore, to obtain the effective dielectric functions, the samples were thoroughly polished by using a colloidal silica polishing suspension (Mastermet). After this treatment, the real and imaginary parts of the dielectric function $\varepsilon(\omega) = \varepsilon_1(\omega) + i\varepsilon_2(\omega)$ have been obtained from the

measured ellipsometric parameters ψ and δ, assuming a two-phase (substrate-ambient) model as reported elsewhere [25].

Figure 3 shows the experimental spectra dependence with energy of the dielectric functions for the polished samples. The structures observed in the ε(ω) spectra are attributed to interband critical points (CPs) which can be analyzed in terms of standard analytic line shapes:

$$\varepsilon(\omega) = C - Ae^{i\phi}(\omega - E + i\Gamma)^m \qquad (1)$$

where A is the amplitude, E is the energy threshold, Γ is the broadening and ϕ is the excitonic phase angle. These parameters are determined by fitting the numerically obtained second derivative spectra $d^2\varepsilon(\omega)/d\omega^2$ of the experimental ε(ω). The exponent m takes the value -1/2 for 1D, 0 (ln(ω-E+iΓ)) for 2D and ½ for 3D CPs. From them, direct information on the energy separation of the VB and CB can be obtained [25]. The spectra exhibit several CPs structures E_0, E_{1A} and E_{1B}, as reported for CZTS [22], CZGS bulk crystals [23] and CZTS thin films [26].

To determine the CP energies, the ε spectra were smoothed with fast Fourier transform filtering before fitting $d^2\varepsilon(\omega)/dE^2$. Second derivatives of complex dielectric function of the polished samples as well as the fittings obtained from the analytical model are represented in Figure 4. These fits agree well with the experimental results and have been obtained considering CPs of 3D-type in the E_0 region and of 2D-type for E_{1A} and E_{1B} regions. The fundamental absorption edge $E_0 = E_g$, the second E_{1A} and third E_{1B} energy thresholds for all the polished crystals are given in Figure 4.

As we mentioned above, the samples were polished to minimize the effects of surface roughness and oxide formation on the determination of the dielectric function. Nevertheless,

the characterization of the surface properties of the as-grown samples is also important to understand how the performance of the solar cells could be affected. Therefore, in order to clarify the chemical nature of the surface of the single crystals, XPS measurements were carried out. Figures 5.a. and 5.b. display the spectral region of Ge *3d* photoemission peak of the samples $CZT_{0.9}G_{0.1}S$-1 and $CZT_{0.5}G_{0.5}S$-2. The Ge *3d* was fitted using two peaks by Voigt functions and a linear background. Figures 5.a. and 5.b. show a clear contribution of GeO_2 at E_B = 32.2 and 32.7 eV for the samples with x = 0.1 (46.9 % of the area) and 0.5 (17.7 % of the area) respectively [27]. The main contribution to the Ge *3d* photoemission peak, at E_B = 30.9 and 31.1 eV for x=0.1 and 0.5 respectively, is assigned to Ge-S bonds in GeS_2, which appears plausible when considering CZTGS as a quaternary Cu_2S-ZnS-SnS_2-GeS_2 system. However, these binding energies are a little bit higher than those reported in [27], which could be explained by different oxidation states of the Ge in CZTGS and GeS_2. Moreover, no ZnO, only very little amounts of Cu_2O and oxidized sulphur (most likely sulphate) were observed. There was no clear evidence of the presence of SnO/SnO_2. In order to clarify the last issue, SnS_2 bulk compound was synthesized in our laboratory. Figure 6 shows the Sn *3d* photoemission peak for the SnS_2 bulk compound, $CZT_{0.9}G_{0.1}S$-1 and $CZT_{0.5}G_{0.5}S$-2 single crystals. As shown, the binding energy of Sn *3d* is different for each compound, decreasing with the increased Ge content. A contribution at E_B = 487.4 eV is only measured for the sample with higher Ge content, and it can be attributed to SnO_2 [27] .The oxygen concentration for the samples with x = 0.1 and 0.5 was 25.2 at % and 19.9 at % respectively, as measured by XPS. A higher concentration of GeO_2 was found for the sample with lower Ge content. This could have been caused by Ge segregation and/or clustering that in turn may lead to an increase of the amount of GeO_2

The optical properties of the as-grown samples (before polishing) were also measured and the results of the corresponding effective dielectric functions are shown in Figure 7. As it can be

seen, they are substantially different from those of the polished samples (Figure 3). In principle, the different dielectric functions lead to corresponding different fundamental band gap energies of the semiconductor, which is very important for the future photovoltaic device. Nevertheless, it is known that the presence of overlayers can also originate these differences.

4. Discussion

The energy threshold of the fundamental absorption edge $E_0 = E_g$ may correspond to a direct transition from the VBM to the CBM. An increase in the E_0 value is clearly observed when x is increased from 0.1 to 0.5. Moreover, a higher E_0 has been also determined for the $CZT_{0.5}G_{0.5}S$-2 sample with lower Cu and Zn contents. Theoretical works suggest that Zn does not play an important role for the determination of the band gap energy [18]. Therefore, this E_0 increase could be mainly associated with the decrease in the Cu content. As mentioned above, the Cu-S d-p coupling determines the VBM level and the Cu-poorer material shows a higher band gap primarily caused by a lowering of the VBM [28-30]. A similar behaviour has been observed in the CIGSe chalcopyrite technology. The formation of a "vacancy compound" for Cu-poorer material has played an important role in high-efficiency solar cells by favourably adjusting the band line-up at the CISe/CdS (p-n) interface [31]. Therefore, the combination of a Ge-graded layer and a Cu-poorer composition could lead to an enhanced efficiency of the photovoltaic devices. In addition, the highest efficiency reported is based on Cu-poor stoichiometry CZTSSe thin films [1].

Following the theoretical calculations, direct band gaps for quaternary germanium (CZGS) kesterite and stannite-type are 2.27 [18]/2.46 [19] eV and 2.06 [18]/2.14 [19] eV respectively. Therefore according to the experimental E_0 values reported in Fig. 4 for our

samples it is most likely that they show a dominant kesterite structure. Indeed, this is confirmed by X-ray diffraction and Raman spectroscopy measurements for the sample with x = 0.1. As shown in Fig. 2, the Raman peaks observed for x = 0.1 are all related to the kesterite structure. All these peaks are shifted towards higher frequencies in comparison to those observed for the CZTS structure [32-33]. This is due to the partial substitution of Sn by Ge [34]. Therefore, the main vibrational A_1 symmetry modes typical for the kesterite structure are detected at 289 and 339 cm^{-1} for x = 0.1 (at 287-288 and 337-338 cm^{-1} for CZTS) [32-33, 35]. For the case of the $CZT_{0.5}G_{0.5}S$-1 the Raman spectrum shows an additional peak at 354 cm^{-1}. A similar peak centered at 360 cm^{-1} was found in orthorhombic stannite CZGS [36]. This new peak may be related to the stannite phase. Therefore for the x = 0.5 sample the kesterite and stanite phases co-exist. It seems that a transition from kesterite to stannite takes place when the Ge concentration increases. Moreover, a decrease in the intensity of the 112 diffraction peak, characteristic of the kesterite structure, for the sample $CZT_{0.5}G_{0.5}S$-1 at around $2\theta = 28.5^{o}$ has been noted (see Fig. 1), which agrees with the possible structure transition.

The second E_{1A} energy threshold appears in the region of 2.75 eV and at around 2.91-3.08 eV for x = 0.1 and 0.5 respectively, while E_{1B} appears in the region of 4.09 eV and 4.11-4.30 eV for x = 0.1 and 0.5 respectively (see Figure 4). Levcenko et al. [22] assigned the E_{1A} and E_{1B} transitions to those at the N point in the Brillouin zone, assuming that the origin of these interband transitions in Cu_2ZnSnS_4 is the same as in $CuInS_2$. Later, from first principles calculations [18] and experimental values [23], E_{1A} and E_{1B} have been attributed to transitions at the high CPs N(A): $2\pi/a(0.5\ 0.5\ 0.5)$ and T(Z): $2\pi/a(0\ 0\ 0.5)$ of the first Brillouin zone for the CZGS compound. Band structure calculations are necessary to identify the energy transitions observed experimentally for the alloying CZTGS, but the same behaviour could be expected.

By using the information given by XPS, we studied in more detail the optical response of the as-grown samples. For this purpose a three-layer model was considered, i.e. substrate/overlayer/ambient. The overlayer thickness was assumed to be in the 10 nm range and the effective dielectric constants of the overlayer were modelled using an effective medium approximation (EMA). The composition of the layer was varied in order to fit the experimental ellipsometric spectra of the unpolished samples. For the substrate, i.e. the bulk sample, we have used the dielectric constants (ε) shown in Figure 3. Figure 7 shows the good agreement that is obtained between experimental and calculated values using the EMA model based on a mixed of different layers: bulk compound corresponding to the polished sample, 55% GeO_2, 5% SnO_2/Cu_2O and 40 % voids on the surface. To achieve the fit, the optical constants of GeO_2 [37], SnO_2 [38] and Cu_2O [39] were introduced in the model. Note that also a void fraction is included to take into account the sample roughness. Different EMA models were used and compared for the sample $CZT_{0.5}G_{0.5}S$-2 (see Figure 7.b.). They show two important features: (1) the main oxide phase present is GeO_2, although the fit is improved slightly when a small amount of SnO_2 is also considered, (2) the roughness of the samples plays an important role in the ultraviolet region for energies higher than 2.5 eV approximately. Nevertheless, the latter does not affect the spectra in the region of the fundamental band gap, and thus it does not affect the evaluation of the E_0 value.

4. Conclusions

$Cu_2ZnSn_{1-x}Ge_xS_4$ (x = 0.1, 0.5) single crystals were synthesized by chemical vapour transport. This work shows the potential of the band-gap engineering of $Cu_2ZnSn_{1-x}Ge_xS_4$ as a function of the Ge concentration. The modification of the energy transitions of CZTS alloying with Ge opens an interesting perspective for the enhancement of the transport and

collection of photo-generated carriers of CZTGS-based solar cells. Moreover, the increased E_0 for Cu-poorer CZTGS shows a possible way to adjust the p-n alignment of the photovoltaic devices. On the other hand, the formation of GeO_2 on the surface of these compounds has been demonstrated by XPS measurements. This should be taken into account when designing and fabricating solar cells since it modifies the values of the effective transition energies. This fact stresses the relevance of the surface preparation of the CZTGS material, which is extremely important to enhance the p-n heterointerface of the solar cell devices.

Acknowledgments

RC acknowledges financial support from Spanish MINECO within the program Ramón y Cajal (RYC-2011-08521). This work was supported by the Marie Curie-IRSES project (PVICOKEST, GA: 269167), MINECO projects (KEST-PV, ENE2010-21541-C03-01/-02/-03) and Marie Curie-ITN project (KESTCELL, GA: 316488).

References

[1] Wang W, Winkler MT, Gunawan O, Gokmen T, Todorov TK, Zhu Y, Mitzi DB, Adv. Energy Mater **2013**, DOI: 10.1002/aenm.201301465.

[2] Todorov TK, Tang J, Bag S, Gunawan O, Gokmen T, Zhu Y, Mitzi DB, Adv. Energy Mater. 2013;3: 34.

[3] Katagiri H, Jimbo K, Yamada S, Kamimura T, Maw WS, Fukano T, Ito T, Motohiro T, Appl. Phys. Express 2008;1: 041201.

[4] Repins I, Beall C, Vora N, DeHart C, Kuciauskas D,Dippo P, To B, Mann J, Hsu WC, Goodrich A, Noufi R, Sol. Energy Mater. Sol. Cells 2012;101:154.

[5] Ford GM, Guo Q, Agrawal R, Hillhouse HW, Chem. Mater. 2011;23:2626.

[6] Kato T, Hiroi H, Sakai N, Muraoka S, Sugimoto H, Characterization of front and back interfaces on Cu_2ZnSnS_4 thin film solar cells, in: 27th EPVSEC, 2012, Frankfurt, Germany, pp. 2236-2239.

[7] Shin B, Gunawan O, Zhu Y, Bojarczuk NA, Chey SJ, Guha S, Prog. Photovolt: Res. Appl. 2013;21:72.

[8] Scragg JJ, Kubart T, Wätjen JT, Ericson T, Linnarsson MK, Plätzer-Björkmann Ch, Chem. Mater 2013:25;3162.

[9] Fairbrother A, Fontané X, Izquierdo-Roca V, Espíndola-Rodríguez M, López-Marino S, Placidi M, Calvo-Barrio L, Pérez-Rodríguez A, Saucedo E, Sol. Energy Mater. Sol. Cells 2013;112:97.

[10] Redinger A, Berg DM, Dale PJ, Siebentritt S, J. Am. Chem. Soc. 2011;133:3320. (2011) 3320-3323.

[11] Caballero R, Izquierdo-Roca V, Merino JM, Friedrich EJ, Climent-Font A, Saucedo E, Pérez-Rodríguez A, León M, Thin Solid Films 2013;535:62.

[12] Schockley W, Queisser HJ, J. Appl. Phys. 1961;32:510.

[13] ZSW press release 23.10.2013, http://www.zsw-bw.de/uploads/media/pi18-2013-ZSW-WeltrekordCIGS.pdf

[14] Gabor AM, Tuttle JR, Albin DS, Contreras MA, Noufi R, Hermann AM, Appl. Phys. Letters 1994;65:198.

[15] Chirila A, Buecheler S, Pianezzi F, Bloesch P, Gretener Ch, Uhl AR, Fella C, Kranz L, Perrenoud J, Seyrling S, Verma R, Nishiwaki S, Romanyuk YE, Bilger G, Tiwari AN, Nature Materials 2011;10:857.

[16] Caballero R, Kaufmann CA, Efimova V, Rissom T, Hoffmann V, Schock HW, Prog. Photovolt: Res. Appl. 2013;21:30.

[17] Siebentritt S, Schorr S, Prog. Photovolt: Res. Appl. 2012;20:512.

[18] Chen S, Gong XG, Walsh A, Wei SH, Phys. Rev. B 2009;79: 165211.

[19] Chen D, Ravindra NM, J. Alloys and Compounds 2013;579:468.

[20] Guo Q, Ford GM, Yang WC, Hages CJ, Hillhouse HW, Agrawal R, Sol. Energy Mater. and Sol. Cells 2012;105:132.

[21] Bodnar IV, Inorganic Materials 2002;38:647.

[22] Levcenko S, Gurieva G, Guc M, Nateprov A, Moldavian J. of Phys. Sciences 2009;8:173.

[23] León M, Levcenko S, Serna R, Gurieva G, Nateprov A, Merino JM, Friedrich EJ, Fillat U, Schorr S, Arushanov E, J. Appl. Phys. 2010;108: 093502.

[24] Albornoz JG, Serna R, León M,. J. Appl. Phys. 2005;97: 103515.

[25] Lautenschlager P, Garriga M, Logothetidis S, Cardona M, Phys. Rev. B 1987;35:9174.

[26] Li J, Du H, Yarbrough J, Norman A, Jones K, Teeter G,Terry Jr. FL, Levi D, Optics Express 2012;20: A327.

[27] NIST X-Ray Photoelectron Spectroscopy Database, NIST Standard Reference Database 20, Version 4.1. (http://srdata.nist.gov/xps/).

[28] Han SH, Hasoon FS, Pankow JW, Appl. Phys. Lett. 2005;87:151904.

[29] Han SH, Hermann AM, Hasoon FS, Al-Thani HA, Levi DH, Appl. Phys. Lett. 2004;85: 576.

[30] Levcenko S, Léon M, Gurieva G, Serna R,Merino JM, Friedrich EJ, Arushanov E, Bodnar IV, Materials Chemistry and Physics 2011;125: 77.

[31] Schmid D, Ruckh M, Grunwald F, Schock HW, J. Appl. Phys. 1993;73:2902

[32] Fontané X, Izquierdo-Roca V, Saucedo E, Schorr S, Yukhymchuk VO, Valakh MYa, et al. J Alloys Compd 2012;539:190.

[33] Caballero R, Garcia-Llamas E, Merino JM, León M, Babichuk I, Dzhagan V, Strelchuk V, Valakh M, Acta Materialia 2014;65:412.

[34] Levcenko S, Guc M, Merschjann C, Gurieva G, Schorr S, Lux-Steiner M, Arushanov E, Phys. Stat. Solidi C 2013;10:1079.

[35] M. Dimitrievskaa, A. Fairbrother, A. Pérez-Rodríguez, E. Saucedo, V. Izquierdo-Roca, Acta Materialia 2014;70:272.

[36] Guc M, Izquierdo-Roca V, Pérez-Rodríguez A, Gurieva G, Levcenko S, Schorr S, Arushanov E, Phys. Stat. Solidi C 2013, DOI: 10.10021pssc.

[37] Vega F, de Sande JCG, Afonso CN, Ortega C, Siejka J, Appl. Optics 1994;33:1203.

[38] Paulson PD, Hegedus SS, J. Appl. Phys. 2004;96:5469.

[39] Ribing AG, Roos A, Handbook of Optical Constants II, pp. 880-882, Ed. by E.D. Palik, Academic Press Inc. 1991.

Figure Captions

Figure 1. Powder X-ray diffraction of the $CZT_{0.9}G_{0.1}S$-1 and $CZT_{0.5}G_{0.5}S$-1 compounds. CZTS and CZGS JCPDS references are shown for comparison.

Figure 2. Raman spectra of $CZT_{0.9}G_{0.1}S$-1 and $CZT_{0.5}G_{0.5}S$-1 single crystals. Lorenztian fits and a linear background have been carried out to determine the Raman peaks position.

Figure 3. Dielectric functions of polished CZTGS single crystals. The spectra exhibit three CPs structures E_0, E_{1A} and E_{1B}.

Figure 4. Second derivative spectra of the experimental real and imaginary dielectric functions and the fits based on the Eq. (1) to deduce the transition energies.

Figure 5. Ge*3d* photoemission peak of the samples (a) $CZT_{0.9}G_{0.1}S$-1 and (b) $CZT_{0.5}G_{0.5}S$-2. MgK_{α} excitation is used.

Figure 6. Comparison of the Sn*3d* photoemission peak of SnS_2 bulk compound, $CZT_{0.9}G_{0.1}S$-1 and $CZT_{0.5}G_{0.5}S$-2 single crystals. MgK_{α} excitation is used.

Figure 7. EMA models used to fit the real and imaginary dielectric functions of the unpolished (a) $CZT_{0.9}G_{0.1}S$-1 and (b) $CZT_{0.5}G_{0.5}S$-2 samples.

Table 1. Composition of the single crystals measured by EDX.

Sample	Cu (at%)	Zn (at%)	Sn (at%)	Ge (at%)	S (at%)	Cu/(Zn+IV)	(Cu+Zn)/IV	x	S/M
$CZT_{0.9}G_{0.1}S$-1	24.77	13.13	11.29	1.04	49.77	0.97	3.07	0.08	0.99
$CZT_{0.5}G_{0.5}S$-1	24.29	12.68	6.18	6.14	50.72	0.97	3.00	0.50	1.03
$CZT_{0.5}G_{0.5}S$-2	22.11	11.11	6.63	5.58	54.28	0.94	2.72	0.46	1.19

Note: M= Cu + Zn + Sn + Ge; IV = Sn + Ge

Figure 1

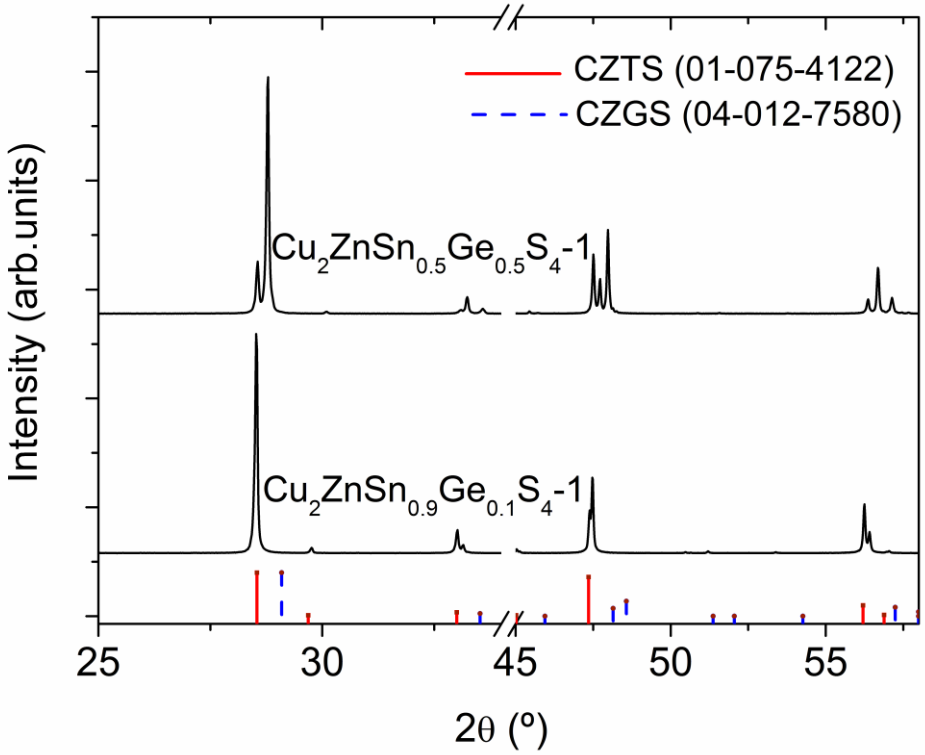
CZTS (01-075-4122)
CZGS (04-012-7580)
Cu2ZnSn0.5Ge0.5S4-1
Cu2ZnSn0.9Ge0.1S4-1
Intensity (arb.units)
25
30
45
50
55
2θ (º)

Figure 2a

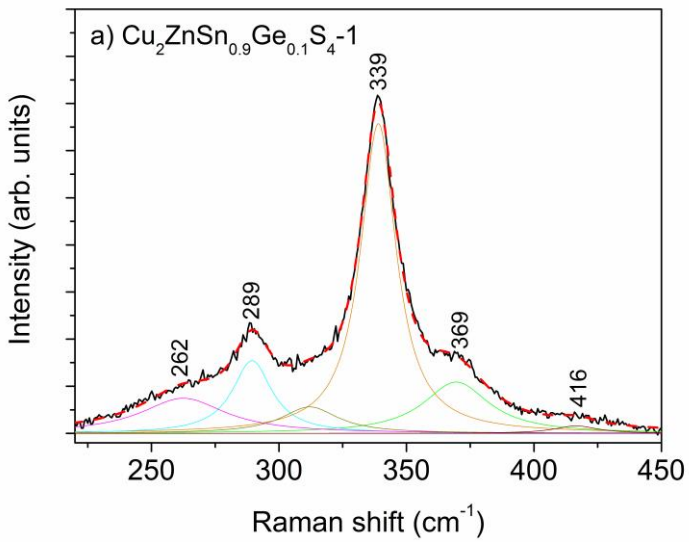

Figure 2b

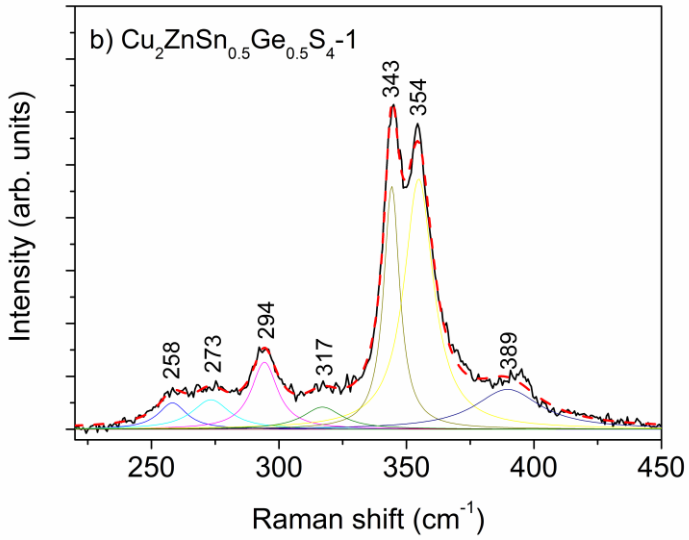

Figure 3

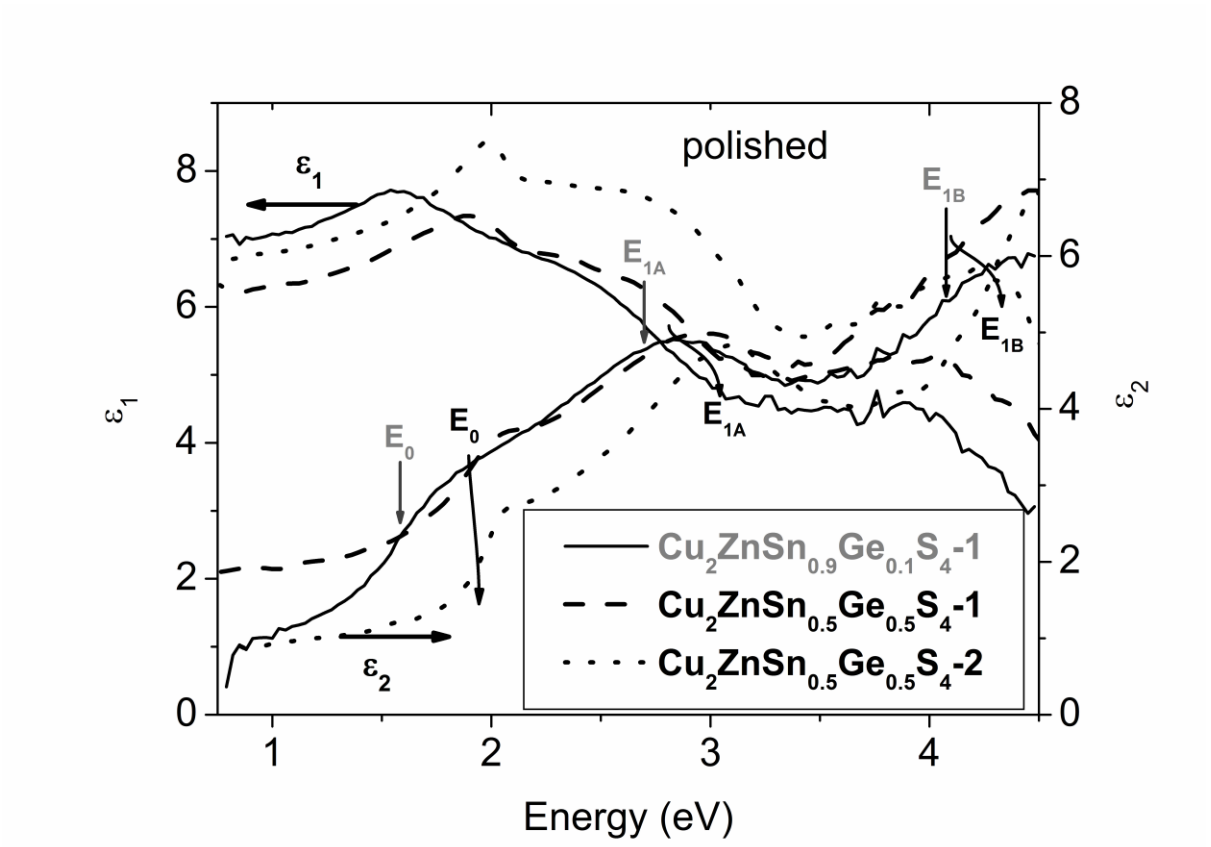
polished
ε1
ε2
E0
E0
E1A
E1A
E1B
E1B
Cu2ZnSn0.9Ge0.1S4-1
Cu2ZnSn0.5Ge0.5S4-1
Cu2ZnSn0.5Ge0.5S4-2
Energy (eV)
ε1
ε2
0
2
4
6
8
1
2
3
4

Figure 4

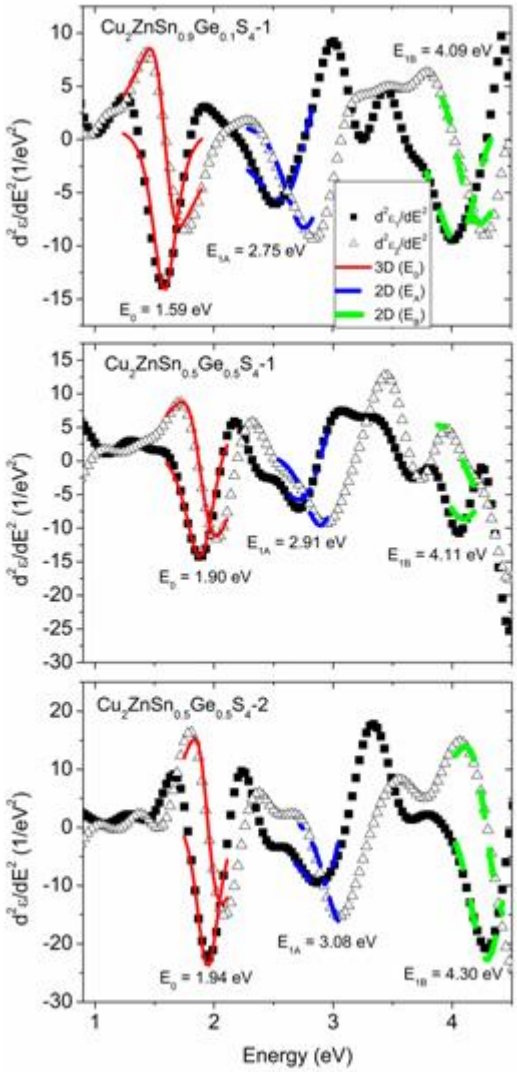
Cu2ZnSn0.9Ge0.1S4-1
E1B = 4.09 eV
E1A = 2.75 eV
E0 = 1.59 eV
d2ε1/dE2
d2ε2/dE2
3D (E0)
2D (E1A)
2D (E1B)
Cu2ZnSn0.5Ge0.5S4-1
E1A = 2.91 eV
E1B = 4.11 eV
E0 = 1.90 eV
Cu2ZnSn0.5Ge0.5S4-2
E1A = 3.08 eV
E0 = 1.94 eV
E1B = 4.30 eV
d2ε/dE2 (1/eV2)
Energy (eV)

Figure 5

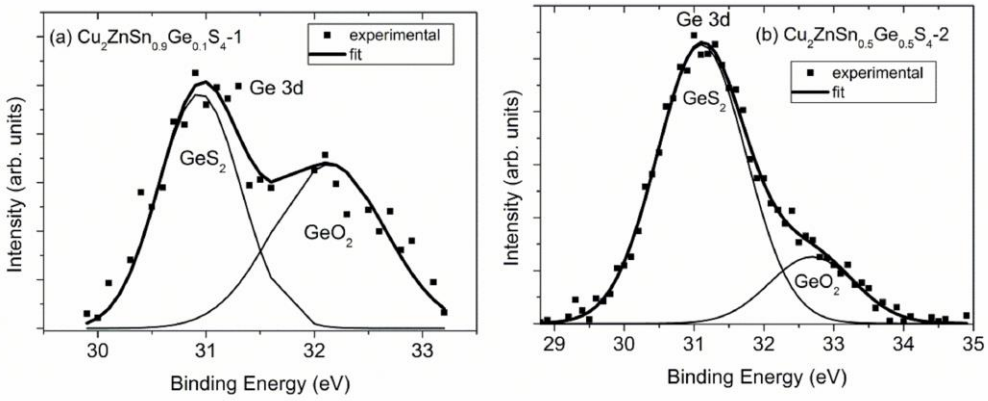
(a) $Cu_2ZnSn_{0.9}Ge_{0.1}S_4$-1
experimental
fit
Ge 3d
GeS_2
GeO_2
Intensity (arb. units)
30
31
32
33
Binding Energy (eV)
Ge 3d
(b) $Cu_2ZnSn_{0.5}Ge_{0.5}S_4$-2
experimental
fit
GeS_2
GeO_2
Intensity (arb. units)
29
30
31
32
33
34
35
Binding Energy (eV)

Figure 6

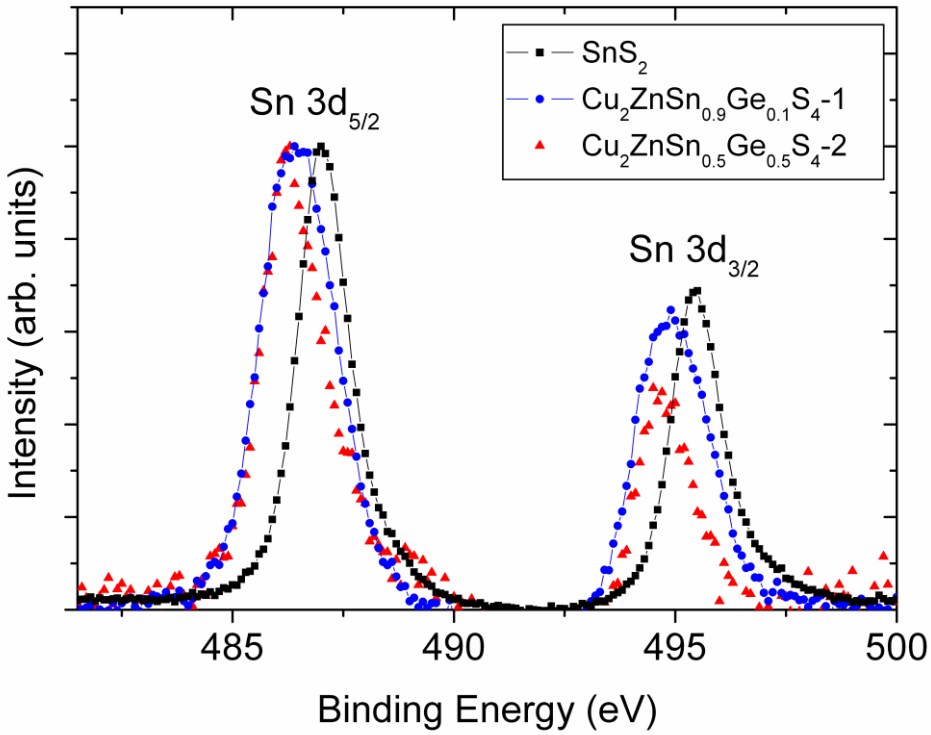
SnS2
Cu2ZnSn0.9Ge0.1S4-1
Cu2ZnSn0.5Ge0.5S4-2
Sn 3d5/2
Sn 3d3/2
Intensity (arb. units)
485
490
495
500
Binding Energy (eV)

Figure 7

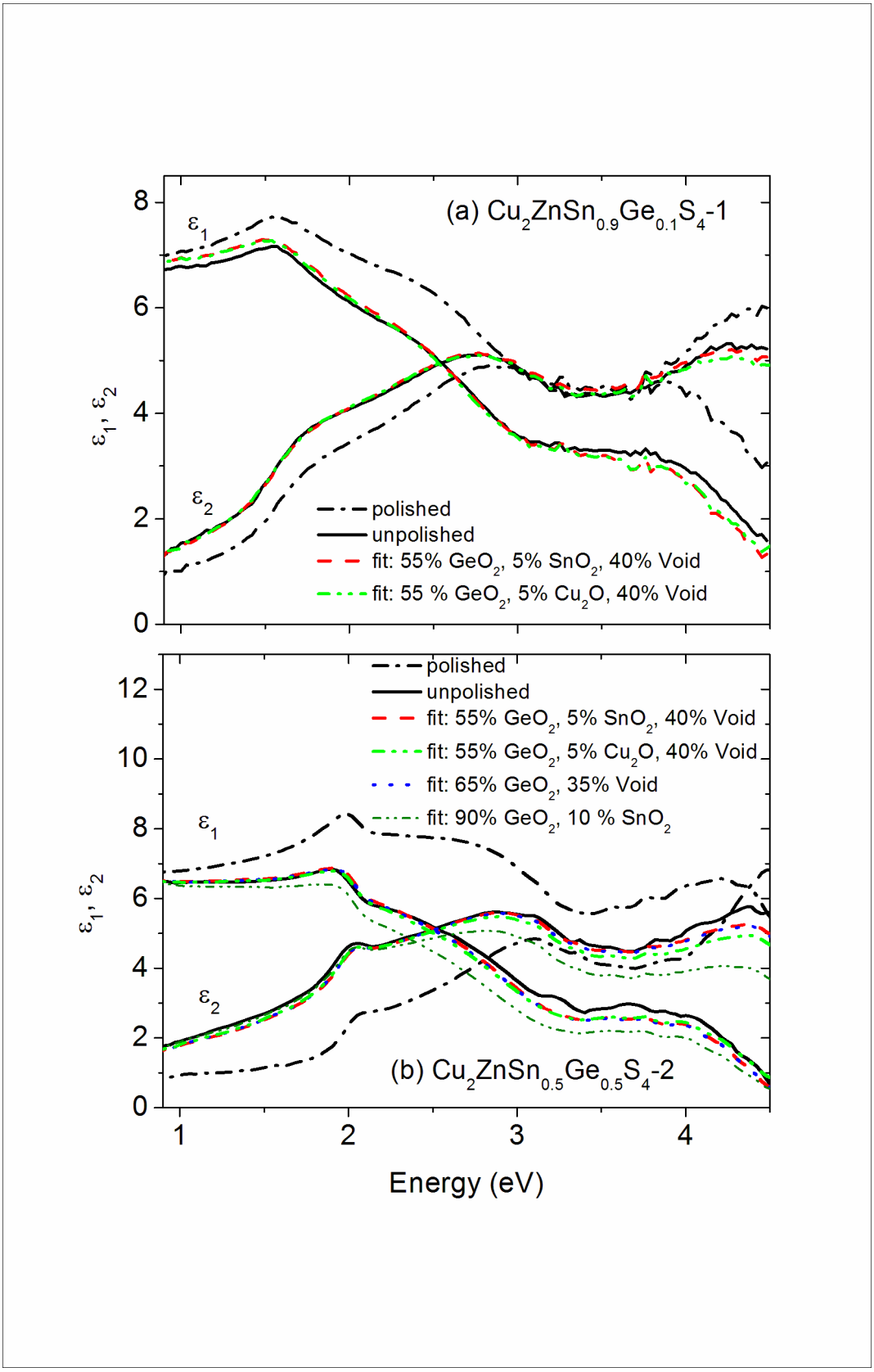
(a) Cu2ZnSn0.9Ge0.1S4-1
ε1
ε2
ε1, ε2
polished
unpolished
fit: 55% GeO2, 5% SnO2, 40% Void
fit: 55 % GeO2, 5% Cu2O, 40% Void
(b) Cu2ZnSn0.5Ge0.5S4-2
fit: 55% GeO2, 5% Cu2O, 40% Void
fit: 65% GeO2, 35% Void
fit: 90% GeO2, 10 % SnO2
Energy (eV)